# Quasiparticle band structure of Zn-IV-$N_2$ compounds

Atchara Punya and Walter R. L. Lambrecht
*Department of Physics, Case Western Reserve University, Cleveland, Ohio 44106-7079*

Mark van Schilfgaarde
*School of Materials, Arizona State University, Tempe, Arizona 85284*

(Received 13 July 2011; published 7 October 2011)

Electronic energy-band structures of the Zn-IV-$N_2$ compounds, with IV equal to Si, Ge, and Sn calculated in the quasiparticle self-consistent GW approximation and using the full-potential linearized muffin-tin orbital approach, are presented. A comparison is made with local-density approximation results. The bands near the gap are fitted to an effective Kohn-Luttinger-type Hamiltonian appropriate for the orthorhombic symmetry, and conduction-band effective masses are presented. Exciton binding energies and zero-point motion corrections to the gaps are estimated. While $ZnSiN_2$ is found to be an indirect gap semiconductor, $ZnGeN_2$ and $ZnSnN_2$ are direct gap semiconductors. The gaps range from the orange-red to deep UV. The valence-band maximum is split in three levels of different symmetry, even in the absence of spin-orbit coupling, and should show transitions to the conduction band, each for a separate polarization. Spin-orbit effects are found to be surprisingly small, indicating almost exact compensation of the N-2$p$ and Zn-3$d$ contributions.

DOI: 10.1103/PhysRevB.84.165204 PACS number(s): 71.20.Nr, 71.15.Nc

## I. INTRODUCTION

The II-IV-$N_2$ compounds are closely related to the group-III-N semiconductors. They are obtained by replacing the group-III element alternately by a group II, such as Zn, and a group IV, such as Si, Ge, and Sn. While this type of chemical substitution is well known for other group-V semiconductors and transforms the zincblende structure in the chalcopyrite structure, a similar substitution can also be done in the wurtzite structure, commonly found as the lowest-energy crystal structure for the group-III nitrides. As in the chalcopyrite case, it leads to a well-defined ordered crystal structure, with in this case orthorhombic symmetry. This should be contrasted with the substitution of different group-III elements, which usually leads to disordered alloys. We thus call the new compounds heterovalent ternary compounds. Because of their close relation to the group-III-nitrides, one may expect similar but not identical properties. This provides an alternative opportunity for band-structure and other property engineering to the usual III-N alloys.

Nitride compounds of this type have been known since the 1970s but the literature on them is still rather sparse. The earliest report on the synthesis of $ZnGeN_2$ is by Maunaye and Lang in 1970[1] and used a reaction of $NH_3$ with $Zn_2GeO_4$, the latter being separately obtained from reacting $GeO_2$ with ZnO. The initial reports on the crystal structure showed it to have a structure related to that of wurtzite but with a lower, monoclinic symmetry. Because of the closeness in electron density and hence x-ray and electron-scattering factors between Zn and Ge, it was impossible using x-ray diffraction to determine whether the Zn and Ge atoms were ordered or disordered on the cation lattice. A neutron-diffraction study[2] determined the ordering of the Zn and Ge atoms and thus established the orthorhombic structure explained in more detail below.

Larson *et al.*[3] used a vapor growth method for $ZnGeN_2$ starting from elemental Zn and Ge in $NH_3$ and reported an absorption onset at 2.67 eV, which is probably an underestimate resulting from defects. High-pressure synthesis of $ZnGeN_2$ and $ZnSiN_2$ starting from mixtures of $Zn_3N_2$ and $Si_3N_4$ or $Ge_3N_4$ was reported by Endo *et al.*[4] They reported a band gap of 3.64 eV for $ZnSiN_2$ based on the optical-absorption onset.

Metal-organic chemical vapor deposition (MOCVD) was used by Zhu *et al.*[5] to synthesize thin films of $ZnGeN_2$. The same group also reported $ZnSiN_2$ growth and alloy growth of $ZnSi_{1-x}Ge_xN_2$ growth, and these materials were investigated by a number of other collaborators determining optical properties,[6,7] transistor devices on SiC,[8] and even their suitability as magnetic semiconductor hosts by implantation of Mn.[9] Muth *et al.*[6] determined band gaps from optical-absorption data as a function of alloy composition in $ZnSi_{1-x}Ge_xN_2$ and found it to vary between $3.1 - 3.2$ eV for $ZnGeN_2$ and 4.4 eV in $ZnSiN_2$. Cook *et al.*[7] determined the indices of refraction and Mintairov *et al.*[10] determined the infrared reflection relating to the vibrational spectrum.

Misaki *et al.*[11–13] used remote plasma-enhanced MOCVD for thin-film growth of $ZnGeN_2$ and reported a band gap of 3.3 eV. They also reported optical reflectivity in the UV up to 20 eV. Most of this work used r-plane sapphire as the substrate. Cloitre *et al.* reported $ZnSiN_2$ growth by Metal-organic vapor phase epitaxy on c-plane sapphire.[14] Kikkawa and Morisaka[15] reported Radio Frequency (RF)-sputter deposition of $ZnGeN_2$ thin films on Si and glass substrates and estimated the gap to be about 3.1 eV. Viennois *et al.*[16] performed the first Raman spectroscopy study on powder samples of $ZnGeN_2$, synthesized by a similar approach to that used by Maunaye and Lang.

Recently a vapor-liquid-solid-synthesis method was used by Du *et al.*[17] using pure Zn and Ge, and $NH_3$, at growth temperatures between 750 and 900 °C. Photoluminescence on these materials indicates a gap of $3.40 \pm 0.01$ eV and a high ratio of band-gap versus defect luminescence.

The first band-structure calculations of $ZnGeN_2$ were presented in 1999 by Limpijumnong *et al.*[18] using the local-density approximation and linearized muffin-tin orbital method. They also investigated the linear and nonlinear

 

optical properties such as the index of refraction and second-harmonic generation coefficient. Other groups also presented band-structure calculations with pseudopotential plane-wave approaches[19,20] and included some other members of this family of II-IV-$N_2$ compounds.

Recently, Lambrecht *et al.*[21–25] presented a series of papers mainly focusing on the lattice dynamics of $ZnSiN_2$, $ZnGeN_2$, and $ZnSnN_2$. As part of this work, the electronic band structures were also calculated using a pseudopotential plane-wave approach.[26] All of these previous works on the band structure, however, suffer from the limitations of the local-density approximation. Although some earlier estimates of the band gaps going beyond LDA were mentioned in Paudel and Lambrecht,[24] there is still considerable uncertainty on the band structures both from the theoretical and experimental point of view.

In this paper we present quasiparticle self-consistent GW (QSGW) calculations of the band structures of $ZnSiN_2$, $ZnGeN_2$, and $ZnSnN_2$. The QSGW method has been shown to provide reliable predictions of the band gaps of a large variety of semiconductors.[27] The calculations are performed using an accurate full-potential linearized muffin-tin orbital method.[28,29] The crystal structure and symmetry are discussed first. We re-optimized crystal structure parameters using the full-potential linearized muffin-tin orbital (FP-LMTO) method in the local density approximation before proceeding with the GW calculations. After a discussion of the differences between local-density approximation (LDA) and GW and the atomic-orbital character of the energy bands over a wide energy range, we focus on the region near the band gap. Besides the band gaps, it is of interest to determine some details of the valence-band maximum splittings and the effective masses. We present a generalization of the Kohn-Luttinger Hamiltonian suitable for crystals of orthorhombic symmetry based on the method of invariants and determine the relevant inverse effective mass parameters in this model. We also include and discuss the spin-orbit splittings of the valence-band maximum (VBM). We use our calculated effective masses to estimate exciton binding energies and estimate other corrections to the band gaps such as the zero-point motion electron-phonon renormalization correction.

## II. CRYSTAL STRUCTURE

The prototype for the crystal structure of the II-IV-$N_2$ compounds is $\beta$-$NaFeO_2$, which is actually a I-III-$VI_2$ compound but is related in a similar way to the wurtzite structure of a II-VI compound. This crystal structure can be viewed as a $2 \times \sqrt{3}$ superlattice of wurtzite along orthohexagonal axes as illustrated in Fig. 1 showing a projection on the c plane. It has 16 atoms per unit cell. The $b/a$ and $c/a$ can both adjust as well as the internal positions $x,y,z$ of each of the four types of atoms—the group-II, group-IV, and two inequivalent N positions—$N_{II}$ being on top of the group-II element and $N_{IV}$ being on top of the group-IV element. We choose the $a$ axis to be $2a_w$ and $b \approx \sqrt{3}a_w$, unlike the commonly found choice in the crystallography literature, which interchanges $a$ and $b$ from ours.

The space group is $Pbn2_1$ (space group No. 33, or $C_{2v}^9$), meaning that there is a two-fold screw axis along the $z$ direction

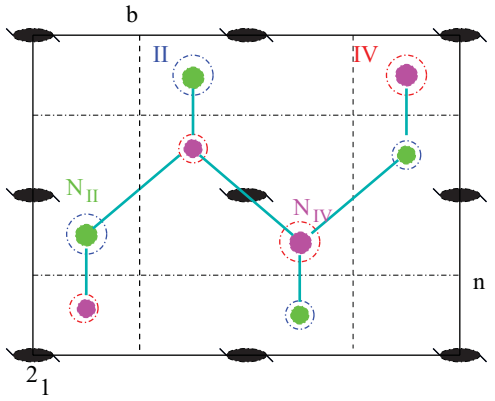


FIG. 1. (Color online) Projection of crystal structure of Zn-IV-$N_2$ compounds on $c$ plane with symmetry elements. Large open circles indicate cations in the bottom plane, small open circles indicate cations in the top plane, and filled circles are N atoms above them as indicated. The symmetry elements are indicated and chosen so that the $2_1$ axis passes through the origin.

with translation $1/2\mathbf{c}$, a diagonal glide plane $n$ perpendicular to $\mathbf{b}$ with translations $1/2(\mathbf{a}+\mathbf{c})$, and an axial glide plane perpendicular to the $a$ axis with translation $1/2\mathbf{b}$. These symmetry elements are indicated in the figure.

The point group is thus $C_{2v}$. The character table for this group was given in Ref. 23. We here just note that the $a_1$, $b_1$, and $b_2$ irreducible representations correspond to $z$, $x$, and $y$ basis functions with $x$ along $a$, $y$ along $b$, and $z$ along the $c$ axes. The $a_2$ irreducible representation is even under the two-fold rotation but odd under both mirror planes and corresponds to an $xy$ basis function.

## III. COMPUTATIONAL METHOD

Density-functional theory in the local-density approximation (LDA) as well as the generalized gradient approximation (GGA)[30] is used to optimize the lattice constants and atomic positions inside the unit cell. These calculations are carried out using a full-potential linearized muffin-tin orbital (FP-LMTO) method.[28,29]

We use a $4 \times 4 \times 4$ k-point sampling for the Brillouin-zone integration in the self-consistent LDA or GGA calculations. The basis set contains two sets of smoothed Hankel function decay parameters $\kappa$ and smoothing radii $R_{sm}$ and includes $spd$ functions in the first and the second set for Zn and includes $spd$ functions in the first and $sp$ in the second set for Si, Ge, Sn, and N. In addition we add Zn-4$d$ as local orbitals.

The quasiparticle band structure is calculated using the quasiparticle self-consistent GW approach implemented in the same FP-LMTO method as described in Refs. 27,31 and 32. In this approach, Hedin's GW approximation[33,34] (GWA) for the self-energy, schematically $\Sigma(12) = iG(12)W(1_+2)$, with $G(12)$ the one-electron Green's function and $W(1_+2)$ the screened Coulomb interaction—written in position, spin, and time coordinates $1 = \{\mathbf{r}_1,\sigma_1,t_1\}$, with $1_+ = t_1 + \delta$—is applied not as a single-shot correction to LDA, as is usual,

but starting from a self-consistently determined static (but nonlocal) exchange-correlation potential:

$$V_{\rm xc}^{\rm QSGW} = \frac{1}{2}\sum_{\rm nm} |\Psi_n\rangle \Re[\Sigma_{\rm nm}(E_n) + \Sigma_{\rm nm}(E_m)]\langle\Psi_m|, \quad (1)$$

Here $\Psi_n$ are the one-electron Kohn Sham eigenstates and $\Re$ means taking the Hermitian part. This approach is designed so that the eigenvalues of the Kohn-Sham independent-particle equations $\epsilon_{n\mathbf{k}}$ approach the quasiparticle energies $E_{n\mathbf{k}}$ in the GWA. $W$ is calculated as $W = (1 - v\Pi)^{-1}v$ and $\Pi(12) = -iG(12)G(21)$ in the random-phase approximation (RPA). A mixed plane-wave and product basis set[35] is used to express all two-particle operators. For details, we refer the reader to the above mentioned papers by the van Schilfgaarde group. Let us here just remark that this method provides very accurate results for a wide range of solids, including all standard III-V and II-VI semiconductors.[31] Most important, the method has highly systematic small remaining errors: it gives a slight overestimate of the gaps compared with the experiment. This remaining discrepancy is thought to arise from the underscreening by the RPA. It can be corrected by scaling the final $\Delta V_{\rm xc} = V_{\rm xc}^{\rm QSGW} - V_{\rm xc}^{\rm LDA}$ by about 80% as obtained empirically by comparing QSGW with the experiment for a wide variety of semiconductors.[31] We refer to this as the $0.8\Sigma$ approximation. Within this approximation most band gaps are obtained to better than 0.1 eV. The $\Delta V_{\rm xc}$ represented in a muffin-tin orbital basis set can be Fourier transformed to real space and then Bloch summed for arbitrary k points on a finer mesh than the one on which the time-consuming GW calculation is carried out. This allows us to obtain accurate effective masses and band plots along symmetry lines.

As explained in Ref. 32 the $\Delta V^{\rm xc}_{\tilde{n}\tilde{m}}(\mathbf{k})$ in the basis set of the LDA Hamiltonian eigenstates (as indicated by the $\tilde{}$ over the indices) can be approximated to be linear in the LDA eigenvalue: $a\epsilon^{\rm LDA}_{\tilde{n}\mathbf{k}} + b$ for energy bands above some cutoff energy $E_{\rm cut}$. We find it is important to take this cutoff sufficiently high for the nitrides, say $E_{\rm cut} = 3$ Ryd above the Fermi level, to obtain well-converged results. The gaps for $E_{\rm cut} = 2.5$ Ryd were still underestimated by 5−10%. As **k**-point sampling set for the GW self-energy we use a $2 \times 2 \times 2$ mesh corresponding to the 16 atom unit cell. This is more or less equivalent to a $8 \times 8 \times 4$ sampling for wurtzite.

## IV. RESULTS

### A. Structural results

The lattice constants obtained by energy minimization in both LDA and GGA are presented in Table I compared with experimental values where available. We note that, even for $ZnGeN_2$, the most studied of these materials, there is still considerable variation between experimental results on the lattice constants obtained from different growth methods, reflecting for example film strain conditions, as discussed in more detail in Du *et al.*,[17] and that $ZnSnN_2$ has not yet been synthesized. For example, Du *et al.*[17] obtain a $b/a_w$ ratio of 1.741 and $c/a_w$ of 1.627 with a lattice constant $a = 6.314$ Å. This gives $V = 178.24$ Å$^3$. We also compare our results with those of a previous calculation by Paudel and Lambrecht[24] The average deviation of the lattice constants from the experiment is most easily seen by comparing the volumes. We see that, as usual, LDA slightly underestimates the volume while GGA overestimates it. For $ZnSiN_2$, GGA appears closer to the experiment, and for $ZnGeN_2$ LDA is slightly closer, but neither has a clear advantage. The ratios $b/a_w$ and $c/a_w$ are slightly larger in our calculated results than in the experiment and LDA seems closer to the experiment for those than GGA. The remaining discrepancies in $b/a_w$ and $c/a_w$ with the experiment are of the order 1%, comparable to the experimental uncertainty. Therefore in the remainder of the paper we will calculate the band structures at the LDA equilibrium lattice parameters. Compared with the pseudopotential plane-wave calculations of Paudel and Lambrecht[24] the present results are slightly closer to the experimental values.

TABLE I. Lattice parameters $a$, $b$, and $c$ (Å), lattice volume $V$ (Å$^3$), the average error with respect to experiment $\{\sigma = [(\delta V/V) - 1]/3\}$, and lattice-constant ratio ($a_w = a/2$) in Zn-IV-$N_2$.

| Compound | | LDA | GGA | LDA-ABINIT [a] | Expt.[b] |
|---|---|---|---|---|---|
| $ZnSiN_2$ | $a$ | 6.08 | 6.16 | 6.01 | 6.18 |
| | $b$ | 5.27 | 5.41 | 5.28 | 5.35 |
| | $c$ | 5.02 | 5.11 | 4.98 | 5.05 |
| | $V$ | 160.85 | 170.29 | 158.02 | 166.97 |
| | $\frac{\delta V}{V}$ | 0.96 | 1.02 | 0.95 | |
| | $\sigma$ | −0.012 | 0.007 | −0.018 | |
| | $b/a_w$ | 1.733 | 1.756 | 1.757 | 1.731 |
| | $c/a_w$ | 1.651 | 1.659 | 1.657 | 1.634 |
| $ZnGeN_2$ | $a$ | 6.38 | 6.42 | 6.33 | 6.44 |
| | $b$ | 5.45 | 5.54 | 5.36 | 5.45 |
| | $c$ | 5.22 | 5.27 | 5.11 | 5.19 |
| | $V$ | 181.50 | 187.44 | 173.38 | 182.16 |
| | $\frac{\delta V}{V}$ | 0.996 | 1.03 | 0.952 | |
| | $\sigma$ | −0.001 | 0.009 | | |
| | $b/a_w$ | 1.708 | 1.726 | 1.693 | 1.693 |
| | $c/a_w$ | 1.636 | 1.641 | 1.614 | 1.612 |
| $ZnSnN_2$ | $a$ | 6.59 | 6.70 | 6.76 | |
| | $b$ | 5.70 | 5.80 | 5.85 | |
| | $c$ | 5.41 | 5.53 | 5.58 | |
| | $V$ | 203.21 | 214.89 | 220.67 | |
| | $b/a_w$ | 1.730 | 1.731 | | |
| | $c/a_w$ | 1.642 | 1.651 | | |

[a]Reference 24.
[b]For $ZnSiN_2$ from Ref. 10, for $ZnGeN_2$ from Ref. 2.

Table II gives the reduced coordinates $(x, y, z)$ of the atomic positions after relaxation. All atoms occur in 4(a) Wyckoff positions: (1) $x, y, z$; (2) $-x, -y, z + (1/2)$; (3) $x + (1/2), -y + (1/2), z$; and (4) $-x + (1/2), y + (1/2), z + (1/2)$. Compared with the results given in Paudel and Lambrecht[24] we here use a different setting of the unit cell with the two-fold screw axes passing through the origin, as recommended in the International Tables of Crystallography. All coordinates are relaxed relative to the position of the two-fold screw axes but one finds generally that the Zn and IV atoms are almost exactly shifted by $0.5\mathbf{a}$ from each other. The relaxation consists mainly in an adjustment of each N atom inside its surrounding tetrahedron, approaching the group-IV atom and moving away from the Zn atom. The average bond-lengths are

TABLE II. Wyckoff 4(a) positions (reduced coordinates) in the unit cell.

| Compound | Atoms | $x$ | $y$ | $z$ |
|---|---|---|---|---|
| $ZnSiN_2$ | Zn | 0.623 | 0.089 | 0.000 |
| | Si | 0.126 | 0.074 | 0.000 |
| | $N_{Si}$ | 0.102 | 0.057 | 0.346 |
| | $N_{Zn}$ | 0.649 | 0.109 | 0.402 |
| $ZnGeN_2$ | Zn | 0.625(0.620)[a] | 0.085(0.083) | 0.000(0.000) |
| | Ge | 0.126(0.125) | 0.079(0.083) | 0.001(0.000) |
| | $N_{Ge}$ | 0.113(0.115) | 0.069(0.070) | 0.360(0.365) |
| | $N_{Zn}$ | 0.637(0.640) | 0.096(0.095) | 0.389(0.385) |
| $ZnSnN_2$ | Zn | 0.626 | 0.084 | 0.000 |
| | Sn | 0.127 | 0.083 | 0.002 |
| | $N_{Sn}$ | 0.125 | 0.081 | 0.377 |
| | $N_{Zn}$ | 0.622 | 0.085 | 0.372 |

[a]For $ZnGeN_2$, the numbers in parentheses are the experimental values from Wintenberger *et al.*[2]

summarized in Table III and are in good agreement with Paudel and Lambrecht[24] and with experimental data for $ZnGeN_2$.

In the process of obtaining the optimum lattice volume, we fitted the Vinet equation of state, given by

$$E(V) = E_0 + \frac{2B_0V_0}{(B_0'-1)^2}\{2 - [5 + 3B_0'((V/V_0)^{1/3} - 1) - 3(V/V_0)^{1/3}]e^{-\frac{3}{2}(B_0'-1)[(V/V_0)^{1/3}-1]}\} \quad (2)$$

to the energy-versus-volume relation and obtained from this fit, values for the bulk modulus $B_0$, its pressure derivative $B_0'$, and the equilibrium volume $V_0$. These are given in Table IV and are in good agreement with Paudel and Lambrecht[24,25] This establishes that our FP-LMTO calculations describe the structure adequately, so we can move on to a study of the electronic band structure in the next section.

### B. Band structures

The LDA and QSGW band structures of $ZnSiN_2$, $ZnGeN_2$, and $ZnSnN_2$ are compared with each other in Fig. 2. Before discussing the differences we discuss the atomic-orbital character of the bands. The bands fall in three regions: the lower valence band, near −15 eV, is the N-2$s$-like band; bands in the range from −5 to 0 eV are mostly N-2$p$, but near 5 eV in LDA and about 2 eV lower in GW we find the Zn-3$d$ bands overlapping with them. The N-2$p$ bands are fairly strongly hybridized with cation $s$ and $p$ orbitals, as can be seen in the partial density of states shown in Fig. 3. A more detailed examination of the orbital character of the conduction-band minimum (CBM) indicates that the CBM has slightly higher group-IV than group-II cation-$s$ character. Thus to maximally change the band gap it is more efficient to vary the group-IV rather than group-II element.

TABLE III. Average bond lengths (Å).

| Compound | Zn-N (Å) | IV-N (Å) |
|---|---|---|
| $ZnSiN_2$ | 2.02 | 1.74 |
| $ZnGeN_2$ | 2.03(2.01)[a] | 1.88(1.88) |
| $ZnSnN_2$ | 2.04 | 2.02 |

[a]Experimental values from Wintenberger *et al.*[2] in parentheses.

TABLE IV. Bulk moduli and their pressure derivatives of Zn-IV-$N_2$ compounds obtained from fit to Vinet equation of state.

| | $B_0$ (GPa) | | $B_0'$ | |
|---|---|---|---|---|
| Compound | LDA | GGA | LDA | GGA |
| $ZnSiN_2$ | 234 (228)[a] | 208 | 4.4 (4.4) | 4.4 |
| $ZnGeN_2$ | 207 (197) | 178 | 4.8 (4.4) | 4.9 |
| $ZnSnN_2$ | 177 (184) | 150 | 4.9 (4.8) | 4.8 |

[a]Values in parentheses from Paudel and Lambrecht.[24]

The band gaps are summarized in Table V. First, we note that $ZnSiN_2$ has an indirect minimum gap slightly lower than the lowest direct gap. All compounds have their conduction-band minimum (CBM) at Γ but the valence-band maximum (VBM) in $ZnSiN_2$ occurs at a point along the Γ–$Y$ direction close to $Y$.

Before comparison with the experiment, we add an estimated zero-point motion band-gap renormalization correction $\Delta(0)$ and exciton binding-energy correction $E_{xb}$. The former were tabulated by Cardona and Thewalt[36] for various semiconductors. We find that for the III-N semiconductors this correction is approximately proportional to the band gap itself and approximately given by $-50 - 31E_g$ meV. This gives $\Delta(0)$ as −227, −162, and −117 meV for $ZnSiN_2$, $ZnGeN_2$, and $ZnSnN_2$, respectively.

The exciton binding energies are estimated from

$$E_{xb} = \frac{\mu}{\varepsilon_0^2}\text{Rydberg}, \quad (3)$$

where we use the reduced mass $\mu = m_cm_v/(m_c + m_v)$, with $m_c$,$m_v$ being a directional averaged conduction and valence-band hole mass as obtained in the next section. We here neglect the interaction of the different valence bands and take only the highest VBM into account (which is justified by the fairly large crystal-field splittings) and average the inverse masses over direction. This gives $m_c$ values of 0.293, 0.185, and 0.141 for $ZnSiN_2$, $ZnGeN_2$, and $ZnSnN_2$, respectively. The corresponding $m_v$ values are 0.520, 0.530, and 0.392 and the reduced exciton masses 0.188, 0.137, 0.104. For $ZnSiN_2$, we use the actual VBM, not at Γ so the exciton binding energy corresponds to the indirect gap. For the direct gap we do not include an exciton binding energy. With high-frequency dielectric constants from Paudel and Lambrecht[24] averaged arithmetically over $x$, $y$, and $z$, we obtain the $\varepsilon_\infty$ value of 5.00, 5.37, and 6.37. This would give exciton binding energies of 102, 64, and 35 meV, respectively. Using static dielectric constants 9.33, 9.70, and 12.71 instead, we would obtain exciton binding energies of 29, 20, and 9 meV. These are comparable to the value in GaN of 25 meV.[37] Since these are smaller than the LO-phonon energies, it makes sense to include the ionic screening. The gaps, including both zero-point motion renormalization correction and exciton binding energy, are given in Table V.

For $ZnGeN_2$, our best converged QSGW calculations overestimate the gap by about 0.5 eV, which is typical for QSGW, while $0.8\Sigma$ is very close to the experimental value and

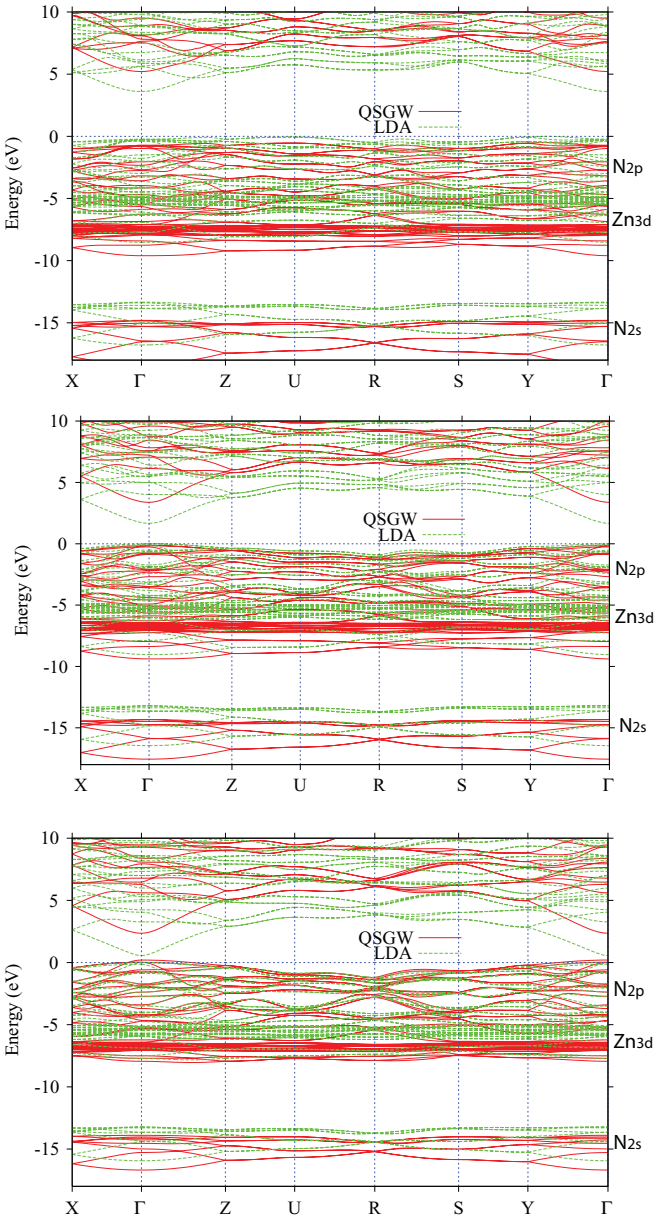


FIG. 2. (Color online) Electronic band structure of $ZnSiN_2$, $ZnGeN_2$, and $ZnSnN_2$.

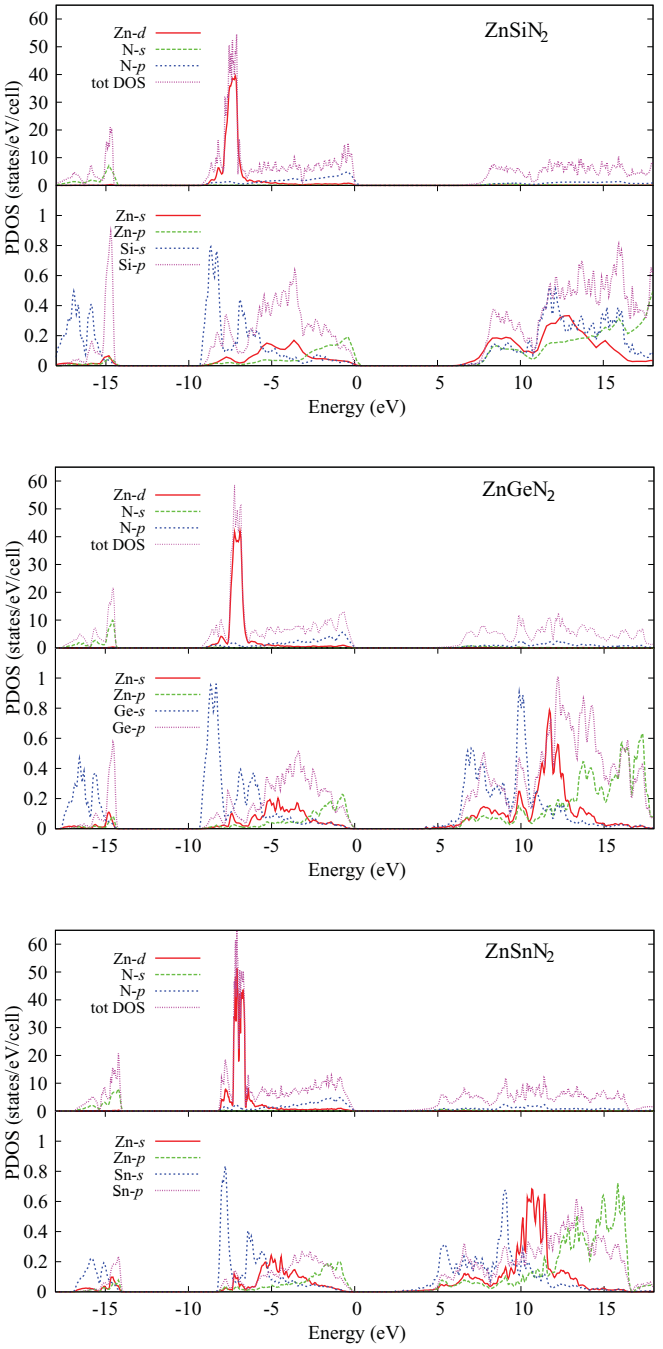


FIG. 3. (Color online) Total and partial densities of states: N-$2s,2p$, IV-$ns,np$, with $n = 3,4,5$ for Si, Ge, Sn, Zn-$4s,4p,3d$, of $ZnSiN_2$, $ZnGeN_2$, and $ZnSnN_2$.

is even closer after adding the above-mentioned corrections. This experimental gap was determined by photoluminescence at 4 K and thus should be very close to our calculated gap. Spin-orbit corrections turn out to be negligibly small for these nitrides, as will be discussed below. The LDA and GGA as usual underestimate the gap significantly. The GGA underestimates it a bit more than LDA, but this is mostly because this calculation was done at the GGA lattice constants, which are slightly larger, and hence the gap is expected to be lower.

For $ZnSiN_2$, even our $0.8\Sigma$ gap is significantly larger than the experimental value. The zero-point motion and exciton binding-energy corrections here are larger, but even so our value is about 1 eV larger than the experimental value. We note, however, that the latter is obtained from absorption measurements at room temperature. The temperature effect could be at most 0.2 eV. So, even taking these corrections into account, there remains a significant discrepancy. Early absorption measurements for $ZnGeN_2$ also gave significantly lower values of the gap, e.g., 2.67 eV in Larson *et al.*,[3] 3.1−3.2 eV,[8] and 3.3 eV.[11] Defect band tails might be responsible for an experimental underestimate of the gap. Earlier work by Endo *et al.*[4] gave an even lower estimate of the onset of absorption in $ZnSiN_2$ of 3.64 eV.

Previous calculations also obtained an indirect gap, for $ZnSiN_2$,[20] of 3.32 eV in LDA. For $ZnGeN_2$ they obtained an LDA gap of 1.67 eV close to ours. The small discrepancy

TABLE V. Band gaps (eV) of Zn-IV-$N_2$ compounds in various approximations.

| Compound | | LDA | GGA | QSGW | $0.8\Sigma$ | $0.8\Sigma + \Delta(0) + E_{xb}$[a] | Expt. |
|---|---|---|---|---|---|---|---|
| $ZnSiN_2$ | Indirect | 3.60 | 3.23 | 6.01 | 5.70 | 5.44 | |
| | Direct | 3.84 | 3.45 | 6.26 | 5.92 | 5.66 | 4.46[b] |
| $ZnGeN_2$ | Direct | 1.66 | 1.57 | 3.99 | 3.60 | 3.42 | 3.40 ± 0.01[c] |
| $ZnSnN_2$ | Direct | 0.55 | 0.35 | 2.64 | 2.15 | 2.02 | |

[a] $\Delta(0)$ is the estimated zero-point motion renormalization correction (see text) and $E_{xb}$ the exciton binding energy.
[b] Osinksy *et al.*[8]
[c] Du *et al.*[17]

in LDA values is likely to arise from the use of different band-structure methods or slightly different lattice constants.

Our predicted gap (including the various corrections) for $ZnSnN_2$ corresponds to a 614-nm wavelength, which is in the orange-red region of the spectrum, while for $ZnGeN_2$ the corresponding wavelength is 362 nm and for $ZnSiN_2$ the indirect and direct gaps correspond to 228 and 218 nm, respectively, well in the UVC range.

Next, we discuss individual band state shifts due to GW. In an electron gas or metal, the GW self-energy $\Sigma_{xc}(\epsilon_F) = 0$ at the Fermi level, and furthermore one knows that near the Fermi level $|\mathrm{Im}\Sigma_{xc}(\omega)| \propto (\omega - \epsilon_F)^2$ and leads to an increasing shift of the levels away from the Fermi level.[34] In a semiconductor we can no longer do this expansion around the Fermi level and the zero of energy of the $\Sigma_{xc}(\omega)$ is set by that of the Green's function of the underlying one-electron Hamiltonian. Although there is no physical meaning to eigenvalues on an absolute scale in a periodic system, we can use the average electrostatic potential as the zero of energy. Quasiparticle shifts of eigenvalues between single-shot GW and the corresponding one-electron Hamiltonian are well defined, because they correspond to the same electron density. We obtain this shift by comparing the QSGW eigenvalues with the LDA eigenvalues obtained with the charge density generated by QSGW. We refer to it as the "pure quasiparticle shift" $\Sigma_i$ for a given level $i$. On the other hand, we can also compare the shifts between the QSGW quasiparticle energies and the LDA eigenvalues for the LDA charge density, where the latter are given with respect to the average electrostatic potential, calculated in the same way by setting the reciprocal lattice vector $\mathbf{G} = 0$ component of the Madelung potential equal to zero. The bands in Fig. 2 were aligned by this procedure. The QSGW and LDA eigenvalues were both determined relative to their average electrostatic potentials and then shifted to the VBM of the LDA as zero of energy. In Table VI, we include both the pure quasiparticle shifts and the shifts between QSGW and LDA. The difference in these two shifts provides an estimate of the error to expect in band offsets from one-shot GW calculations based on the LDA.

TABLE VI. Absolute shifts $(E_i - \epsilon_i)$ (eV) between QSGW and LDA relative to their own average electrostatic potentials and pure quasiparticle shift $\Sigma_i$ (in parentheses) for various levels.

| Level | $ZnSiN_2$ | $ZnGeN_2$ | $ZnSnN_2$ |
|---|---|---|---|
| CBM | 1.6(1.5) | 1.7(1.5) | 1.8(1.6) |
| VBM | −0.5(−0.5) | −0.1(−0.4) | 0.2(−0.3) |
| Zn-3*d* | −2.3(−2.2) | −2.0(−2.0) | −1.5(−1.9) |
| N-2*s* | −1.3(−1.2) | −1.2(−1.1) | −1.0(−0.7) |

These absolute shifts are mainly useful in the context of band-offset calculations between two materials. Once we determine from an interface calculation how the average electrostatic potentials in the two semiconductors are placed relative to each other, and assuming that far away from the interface the material is bulklike, we can then apply the shifts between LDA and QSGW relative to this *local* average electrostatic potential reference and thus obtain a GW correction to the LDA band offset. One can also use core levels or any other "local potential marker" for this purpose, such as the potential at the muffin-tin radius. These shifts also play a role in the understanding of defect levels and alloys.[38]

With these cautions in mind, let us now inspect the results as given in Table VI. We find the pure quasiparticle shifts of the VBM to be negative and those of the CBM to be positive, with the ratio of the CBM shift to the absolute value of the VBM shift increasing from Si to Sn. The dominant shift is always in the CBM. When considering the shifts relative to the pure LDA, which include a change in charge density between LDA and QSGW, we find also a downward shift of the VBM, except for $ZnSnN_2$, for which both the VBM and the CBM shift up relative to LDA. The CBM of $ZnSnN_2$ has a sizeable Sn-*s* contribution. On an absolute scale one expects Sn-*s* levels to lie deeper than, e.g., Ge-*s* levels because *s* levels are nonzero at the nucleus. This is of course the underlying reason for the gap reduction from Si to Ge to Sn. Apparently, for $ZnSnN_2$, the Sn-*s* states are positioned relative to the electrostatic potential reference in such a way as to behave almost like a N-2*p* level, and hence the VBM shift has the same sign as the CBM. The N-2*s* and Zn-3*d* bands shift considerably more down, showing that the GW shifts are orbital dependent: the Zn-3*d* shift down more than the N-2*s* even though the N-2*s* lie below the Zn-3*d*. These average band positions were taken as the peak in the corresponding partial density of states.

### C. Effective valence-band Hamiltonian

In this section, we examine the energy bands near the band gap in more detail. Figure 4 shows the band structures near the the valence-band maximum for the three compounds. The states at Γ are labeled according to the irreducible representations. We note that the conduction-band minimum at Γ has $a_1$ symmetry. Thus direct optical transitions are allowed from $a_1$ to $a_1$ for $\mathbf{E} \parallel \mathbf{c}$, from $b_1$ to $a_1$ for $\mathbf{E} \parallel \mathbf{a}$,

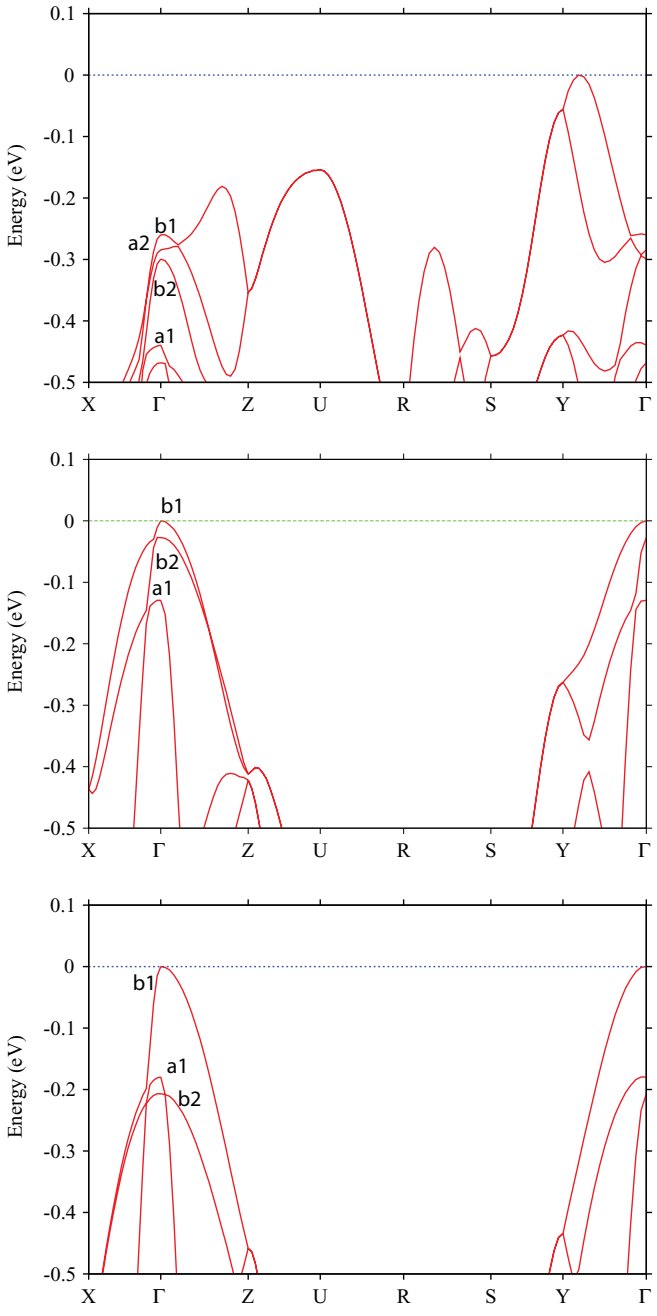


FIG. 4. (Color online) Fine structure of the bands near the valence-band maximum with symmetry labeling at Γ for $ZnSiN_2$, $ZnGeN_2$, and $ZnSnN_2$.

and from $b_2$ to $a_1$ for $\mathbf{E} \parallel \mathbf{b}$. We see that in $ZnGeN_2$ and $ZnSnN_2$ the valence-band maximum is split in three levels even without including spin-orbit coupling. The order of the different symmetry levels is different in each case. In $ZnSiN_2$, in addition, a level of $a_2$ symmetry lies between these levels. This level has no allowed dipole transitions to the CBM. When adding spin-orbit coupling to the calculation, we find almost identical splittings. From the group theory point of view, all transitions then become allowed because all of them belong to the $\Gamma_5$ irreducible representation of the double group, using Koster and Slater's character table. However, the fact that spin-orbit coupling appears to have a negligible effect on the VBM states indicates that we should discuss selection rules based on the single rather than the double group. The selection rules mentioned above imply that these materials might have opportunities for polarization-sensitive detectors. Even for light incident normally to the basal plane, there should be a significant splitting between excitons or light absorbed for the two in-plane polarizations. This results from the low orthorhombic symmetry. At this point, however, no such exciton fine structure has been observed. This will require high-quality films.

The effective masses of the valence bands at Γ are different in each direction $x$, $y$, and $z$ and for each separate valence band. Likewise the CBM has in principle an anisotropic mass tensor with three different diagonal components. The VBM manifold of states can be described by a generalization of the Kohn-Luttinger (for zincblende) or Rashba-Sheka-Pikus (RSP) Hamiltonian for wurtzite. Using the theory of invariants, we can write the effective mass Hamiltonian as follows:

$$\begin{aligned} H^{C_{2v}} &= \Delta_{1c}{L_z}^2 + \Delta_{2c}\left({L_x}^2 - {L_y}^2\right) + \Delta_{1\mathrm{so}} L_z \sigma_z \\ &\quad + \sqrt{2}(\Delta_{2\mathrm{so}} L_x \sigma_x + \Delta_{3\,\mathrm{so}} L_y \sigma_y) \\ &\quad + \left[A_1 + A_2 {L_z}^2 + A_3\left({L_x}^2 - {L_y}^2\right)\right]{k_z}^2 \\ &\quad + \left[B_1 + B_2 {L_z}^2 + B_3\left({L_x}^2 - {L_y}^2\right)\right]\left({k_x}^2 + {k_y}^2\right) \\ &\quad + \left[C_1 + C_2 {L_z}^2 + C_3\left({L_x}^2 - {L_y}^2\right)\right]\left({k_x}^2 - {k_y}^2\right) \\ &\quad + D_1\{L_x, L_y\}k_x k_y + D_2\{L_z, L_x\}k_z k_x \\ &\quad + D_3\{L_z, L_y\}k_z k_y + E_1 L_x k_y + E_2 L_y k_x, \end{aligned} \tag{4}$$

where $\{L_i, L_j\}$ are anticommutators. This includes all terms up to second order that can be formed from the operators $L_i$, $k_i$, and $\sigma_i$ that are invariant (i.e., belong to the $a_1$ representation). At $\mathbf{k} = 0$ we have two crystal-field splittings and three spin-orbit splitting parameters. The remaining terms are inverse effective masses and the parameters $E_1$ and $E_2$ are linear in $k_i$. We have neglected purely relativistic linear terms involving $\sigma_i$ and $k_i$. If $\Delta_{2c} = 0$, $\Delta_{2\mathrm{so}} = \Delta_{3\mathrm{so}}$, $A_3 = 0$, $B_3 = 0$, $C_1 = C_2 = 0$, $C_3 = 2D_1$, $D_2 = D_3$, and $E_1 = E_2$, the above Hamiltonian is reduced to the RSP Hamiltonian valid for $C_{6v}$ symmetry. If we denote the RSP Hamiltonian parameters as defined in Kim *et al.*[39] by $\tilde{A}_i$, we have the relations

$$\begin{aligned} &A_1 = \tilde{A}_1, \quad A_2 = \tilde{A}_3, \quad B_1 = \tilde{A}_2, \quad B_2 = \tilde{A}_4, \\ &C_3 = \tilde{A}_5, \quad D_1 = 2\tilde{A}_5, \quad D_2 = D_3 = \sqrt{2}\tilde{A}_6, \\ &E_1 = -E_2 = \sqrt{2}\tilde{A}_7. \end{aligned} \tag{5}$$

For $\mathbf{k} = 0$ and without spin-orbit splitting, the Hamiltonian in the basis of $Y_l^m$ with $l = 1$ and $m = 1, 0, -1$ is of the form

$$\begin{pmatrix} \Delta_{1c} & & \Delta_{2c} \\ & 0 & \\ \Delta_{2c} & & \Delta_{1c} \end{pmatrix}. \tag{6}$$

The eigenvalues are

$$E_{a_1} = 0, \quad E_{b_2} = \Delta_{1c} + \Delta_{2c}, \quad E_{b_1} = \Delta_{1c} - \Delta_{2c}, \tag{7}$$

where we have used the usual sign convention of the spherical harmonics $Y_1^{\pm 1} = \mp\sqrt{3/8\pi}\sin\theta e^{\pm i\phi}$, so the $x$ orbital, which gives the state with $b_1 = x$ symmetry, corresponds to $-Y_1^1 + Y_1^{-1}$, which indeed corresponds to the eigenvalue with the

− sign in the above equation. Since, in all cases, we find $E_{b_1} > E_{b_2}$, it means that $\Delta_{2c} < 0$. The splittings and $\Delta_{1c}$, $\Delta_{2c}$ parameters are given in Table VIII. We find the hexagonal crystal-field splitting $\Delta_{1c}$ to be significantly larger than in GaN, and furthermore the $\Delta_{2c}$ is of comparable magnitude.

For arbitrary **k** the 3 × 3 Hamiltonian matrix without spin-orbit coupling terms is of the form

$$\begin{pmatrix} \Delta_{1c}+(B_1+B_2+C_1+C_2)k_x^2 \\ +(B_1+B_2-C_1-C_2)k_y^2 \\ +(A_1+A_2)k_z^2 & (D_2k_zk_x-iD_3k_zk_y)/\sqrt{2} \\ & +E_1k_y-iE_2k_x & \Delta_{2c}+(B_3+C_3)k_x^2 \\ & & +(B_3-C_3)k_y^2+A_3k_z^2 \\ & & -iD_1k_xk_y \\ (D_2k_zk_x+iD_3k_zk_y)/\sqrt{2} & & \\ +E_1k_y+iE_2k_x & (B_1+C_1)k_x^2+(B_1-C_1)k_y^2+A_1k_z^2 & (-D_2k_zk_x+iD_3k_zk_y)/\sqrt{2} \\ & & +E_1k_y-iE_2k_x \\ \Delta_{2c}+(B_3+C_3)k_x^2 & & \\ +(B_3-C_3)k_y^2+A_3k_z^2 & (-D_2k_zk_x-iD_3k_zk_y)/\sqrt{2} & \Delta_{1c}+(B_1+B_2+C_1+C_2)k_x^2 \\ +iD_1k_xk_y & +E_1k_y+iE_2k_x & +(B_1+B_2-C_1-C_2)k_y^2 \\ & & +(A_1+A_2)k_z^2 \end{pmatrix}. \quad (8)$$

If we now consider the bands in each of the orthogonal directions, e.g., ($k_x = k_y = 0$), we can diagonalize the Hamiltonian in the same way as for $\mathbf{k} = 0$ and read off the hole inverse masses. We will use the notation $m_\alpha^\lambda$ where λ gives the irreducible representation of the level at Γ and $\alpha$ gives the Cartesian direction $x, y, z$. Thus, we obtain the following relations for the inverse hole masses:

$$\begin{aligned} -\left(m_z^{a_1}\right)^{-1} &= A_1, \quad -\left(m_z^{b_2}\right)^{-1} = A_1+A_2+A_3, \\ -\left(m_z^{b_1}\right)^{-1} &= A_1+A_2-A_3, \quad -\left(m_x^{a_1}\right)^{-1} = B_1+C_1, \\ -\left(m_x^{b_2}\right)^{-1} &= B_1+B_2+B_3+C_1+C_2+C_3, \\ -\left(m_x^{b_1}\right)^{-1} &= B_1+B_2-B_3+C_1+C_2-C_3, \\ -\left(m_y^{a_1}\right)^{-1} &= B_1-C_1, \\ -\left(m_y^{b_2}\right)^{-1} &= B_1+B_2+B_3-C_1-C_2-C_3, \\ -\left(m_y^{b_1}\right)^{-1} &= B_1+B_2-B_3-C_1-C_2+C_3. \end{aligned} \quad (9)$$

In Table VII we summarize the various VBM and CBM effective masses, and in Table VIII we summarize the $A_i, B_i, C_i$ parameters. The remaining parameters $D_i$ only enter if we look at bands in directions intermediate between the in-basal plane and the out-of-basal plane. Assuming the crystal is not too far from hexagonal, which we could call a quasihexagonal approximation, one would have the relation $D_1 = 2C_3$. Furthermore, within the quasicubic relation, one has the approximate relation $\tilde{A}_6 = (4\tilde{A}_5 - \tilde{A}_3)/\sqrt{2}$ in the wurtzite case. This leads here to the relation $D_2 = D_3 = 4C_3 - A_2$. Thus the $D_i$ parameters can be obtained approximately from the ones already determined. The $E_i$ linear in k parameters are related to the anticrossing behavior of the bands one can observe, for example, for the $b_2$ and $a_1$ bands along Γ–$Y$ in $ZnGeN_2$. Since these occur well below the VBM, they are of limited interest and were not determined.

Now, we return to the case $\mathbf{k} = 0$ but add spin-orbit coupling. The 6 × 6 Hamiltonian breaks into two equivalent 3 × 3 Hamiltonians of the form

$$\begin{pmatrix} \Delta_{1c}+\Delta_{so1} & \Delta_{so2}-\Delta_{so3} & \Delta_{2c} \\ \Delta_{so2}-\Delta_{so3} & 0 & \Delta_{so2}+\Delta_{so3} \\ \Delta_{c2} & \Delta_{so2}+\Delta_{so3} & \Delta_{c1}-\Delta_{so1} \end{pmatrix}. \quad (10)$$

The order of the basis function is $m = 1\uparrow$, $m = 0\downarrow$, $m = -1\uparrow$ or equivalently $m = -1\downarrow$, $m = 0\uparrow$, and $m = 1\downarrow$. The eigenvalues are indeed doubly degenerate in spin because of the Kramer's theorem related to time reversal symmetry. If we assume that the spin-orbit coupling parameters are essentially isotropic, $\Delta_{so1} = \Delta_{so2} = \Delta_{so3} = \Delta_s$, which is usually a good approximation because spin-orbit coupling arises from the inner part of the atom where the potential is close to spherically symmetric, we can make some progress by first applying the

TABLE VII. Effective masses (units of free-electron mass $m_e$).

| | | $ZnSiN_2$ | $ZnGeN_2$ | $ZnSnN_2$ |
|---|---|---|---|---|
| CBM at Γ | $m_x^c$ | 0.30 | 0.22 | 0.16 |
| | $m_y^c$ | 0.47 | 0.20 | 0.15 |
| | $m_z^c$ | 0.21 | 0.15 | 0.12 |
| VBM at Γ | $m_x^{a_1}$ | 4.80 | 1.90 | 1.79 |
| | $m_y^{a_1}$ | 0.80 | 2.02 | 1.98 |
| | $m_z^{a_1}$ | 0.21 | 0.15 | 0.12 |
| | $m_x^{b_1}$ | 0.37 | 0.21 | 0.15 |
| | $m_y^{b_1}$ | 4.80 | 2.19 | 2.02 |
| | $m_z^{b_1}$ | 2.97 | 2.26 | 2.04 |
| | $m_x^{b_2}$ | 0.31 | 2.91 | 2.27 |
| | $m_y^{b_2}$ | 1.06 | 0.19 | 0.15 |
| | $m_z^{b_2}$ | 1.18 | 2.42 | 2.34 |
| Actual VBM | $m_x^v$ | 0.55 | | |
| in $ZnSiN_2$ | $m_y^v$ | 0.33 | | |
| | $m_z^v$ | 1.09 | | |

TABLE VIII. Parameters of effective Hamiltonian: inverse mass ($\hbar^2/2m_e$), energy splitting (meV).

| Parameter | $ZnSiN_2$ | $ZnGeN_2$ | $ZnSnN_2$ | GaN |
|---|---|---|---|---|
| $A_1$ | −4.71 | −6.87 | −8.57 | −6.4 |
| $A_2$ | 4.11 | 6.44 | 8.10 | 5.9 |
| $A_3$ | −0.26 | 0.01 | 0.02 | |
| $B_1$ | 0.73 | −0.51 | −0.53 | −0.50 |
| $B_2$ | −1.93 | −2.19 | −3.12 | −2.55 |
| $B_3$ | 0.04 | 0.09 | 0.11 | |
| $C_1$ | −0.52 | −0.02 | −0.03 | |
| $C_2$ | −1.26 | −0.05 | −0.05 | |
| $C_3$ | −0.32 | 2.30 | 3.18 | 2.56 |
| $D_1$ | −0.64 | 4.60 | 6.36 | 5.12 |
| $D_2$,$D_3$ | −5.41 | 2.76 | 4.62 | 4.33 |
| $\Delta_{1c}$ | 160 | 115 | 82 | 36 |
| $\Delta_{2c}$ | −20 | −14 | −94 | 0 |

unitary transformation that diagonalized the matrix without spin-orbit coupling. This leads to

$$\begin{pmatrix} \Delta_{c1}+\Delta_{c2} & \sqrt{2}\Delta_s & \Delta_s \\ \sqrt{2}\Delta_s & 0 & -\sqrt{2}\Delta_s \\ \Delta_s & -\sqrt{2}\Delta_s & \Delta_{c_1}-\Delta_{c2} \end{pmatrix}. \tag{11}$$

If we furthermore assume that the spin-orbit parameter is small compared with the crystal-field splitting of the levels, then in second-order perturbation theory we obtain

$$\begin{aligned} E_{a1} &= -\frac{2\Delta_s^2}{\Delta_{c1}+\Delta_{c2}}, \\ E_{b2} &= \Delta_{c1}+\Delta_{c2}+\frac{2\Delta_s^2}{\Delta_{c1}+\Delta_{c2}}+\frac{\Delta_s^2}{2\Delta_{c2}}, \\ E_{b1} &= \Delta_{c1}-\Delta_{c2}+\frac{2\Delta_s^2}{\Delta_{c1}-\Delta_{c2}}-\frac{\Delta_s^2}{2\Delta_{c2}}. \end{aligned} \tag{12}$$

Strictly speaking, all levels have symmetry $\Gamma_5$ but we still label them by the single group label from which they are derived.

We carried out calculations including spin-orbit coupling and found that the splittings were essentially indistinguishable from the ones without spin-orbit coupling. This indicates that the spin-orbit coupling parameter is very small in these compounds and makes it at this point unpractical and at the same time unimportant to try to extract these small parameters.

The reason for this small spin-orbit coupling is worth some discussion. For the parent compounds, GaN, we find it is already rather small because (1) the N atom is a low-$Z$ element for which relativistic effects are small and (2) there is a negative contribution from the Ga-3$d$ states lying below the VBM but which are nevertheless somewhat hybridized with the VBM. In $ZnGeN_2$, this negative contribution which now derives from the Zn-3$d$ must be even stronger. In fact, we know that in ZnO the spin-orbit splitting becomes negative.[40] One expects it here to be intermediate between GaN and ZnO because only half the cation sites contribute. The Ge-3$d$ or Sn-4$d$ states lie significantly deeper so that their contribution must be significantly smaller. Apparently, the 3$d$ contribution must almost perfectly cancel the N-2$p$ contribution.

Now for $ZnSiN_2$ the $a_2$ valence band lies between the $b_1$ and $b_2$ bands. Along $\Gamma$–$Z$ the point group of the $k$ point is still $C_{2v}$ so the band emanating from $a_2$ retains $a_2$ symmetry and cannot interact with the other bands. Thus it is indeed seen to cross the $b_1$ band as it disperses upward in energy. Along $\Gamma$–$X$ or $\Gamma$–$Y$ the symmetry group is reduced to a single mirror plane, $\sigma_y$, $\sigma_x$, respectively. Along $\Gamma$–$Y$, for example, $a_1$- and $b_2$-derived bands are both even and $a_2$ and $b_1$ are odd under the $\sigma_x$. Thus one can see an anticrossing behavior of the $a_2$- and $b_1$-derived bands along $\Gamma_Y$. However, the effective Hamiltonian describing the states near $\Gamma$ loses its usefulness. In fact, this Hamiltonian is mostly useful as a starting point for envelope function calculations of nanostructure or shallow acceptor impurities or excitons. But the $\Gamma$-point VBM lies about 0.2 eV below the actual VBM. Thus it is more useful to give the anisotropic effective mass tensor of the VBM at this $k$ point. The latter are also given in Table VII.

Finally, it is instructive to compare these parameters with those in GaN. Using Eq. (5) we can rewrite the RSP parameters of GaN derived in Kim *et al.*[39] in our present orthorhombic notation. These are included in Table VIII as the last column. In that case $E_{b_1} = E_{b_2}$ and the masses in $x$ and $y$ directions are the same. We can see that the inverse mass parameters in GaN are similar to those in $ZnGeN_2$ but the crystal-field splitting is significantly smaller. In fact, the value given here from Kim *et al.*[39] was found to be an overestimate due to the LDA compared with the experiment.

## V. CONCLUSIONS

We presented FP-LMTO LDA and GGA calculations of the crystal structure parameters and QSGW band structures of the Zn-IV-$N_2$ semiconductors with IV equal to Si, Ge, and Sn. Excellent agreement is obtained for the structural parameters with the experiment and previous calculations. As for the band structures, we find $ZnSiN_2$ to be an indirect gap semiconductor while the other two are direct gap semiconductors. The band gaps versus lattice constants are summarized in Fig. 5

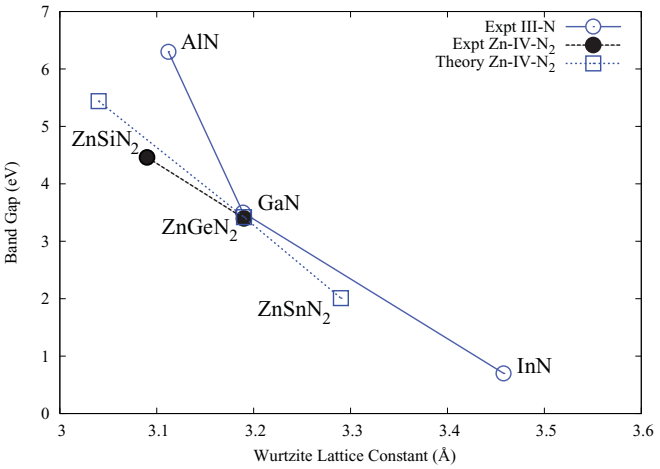


FIG. 5. (Color online) Band gaps as a function of the wurtzite lattice constant of $ZnSiN_2$, $ZnGeN_2$, and $ZnSnN_2$ compared with AlN, GaN, and InN.

compared with the group-III nitride family and firmly establish that these compounds are promising for similar optoelectronic applications as the III-N family. Gap corrections such as exciton binding-energy and zero-point motion phonon renormalization of the gaps were included. Spin-orbit coupling was also taken into account and found to have negligible effect on the valence-band splittings.

The orthorhombic symmetry reduction, compared with the III-nitrides, however, has important consequences in splitting the valence band according to $x, y, z$-like states. The bands near the valence-band maximum were analyzed in detail by generalizing the Kohn-Luttinger Hamiltonian for orthorhombic symmetry, and the corresponding parameters were extracted by fitting to the band structure. Conduction-band masses and exciton reduced masses and binding energies were estimated.

## ACKNOWLEDGMENTS

This work made use of the High Performance Computing Resource in the Core Facility for Advanced Research Computing at Case Western Reserve University and the Ohio Supercomputer Center. The work was supported by the National Science Foundation under Grant No. DMR-0710485.

[1] M. Maunaye and J. Lang, Mater. Res. Bull **5**, 793 (1970).
[2] M. Wintenberger, M. Maunaye, and Y. Laurent, Mat. Res. Bull. **8**, 1049 (1973).
[3] W. L. Larson, H. P. Maruska, and A. Stevenson, J. Electrochem. Soc. **121**, 1683 (1974).
[4] T. Endo, Y. Sato, H. Takizawa, and M. Shimada, J. Mater. Sci. Lett. **11**, 424 (1992).
[5] L. D. Zhu, P. H. Maruska, P. E. Norris, P. W. Yip, and L. O. Bouthillette, in *GaN and Related Alloys*, edited by S. J. Pearton, C. Kuo, A. F. Wright, and T. Uenoyama, Mater. Res. Soc. Proc., Vol. 537 (Materials Research Society, Warrendale, PA, 1999), p. G3.8.
[6] J. Muth, A. Cai, A. Osinsky, H. Everitt, B. Cook, and I. Avrutsky, in *GaN, AlN, InN, and Their Alloys*, Mater. Res. Soc. Symp. Proc., Vol. 831, edited by C. Wetzel, B. Gil, M. Kuzuhara, and M. Manfra (MRS, Pittsburgh, 2005), p. E11.45.1.
[7] B. P. Cook, H. O. Everitt, I. Avrutsky, A. Osinsky, A. Cai, and J. F. Muth, Appl. Phys. Lett. **86**, 121906 (2005).
[8] A. Osinsky, V. Fuflyigin, L. D. Zhu, A. B. Goulakov, J. W. Graff, and E. F. Schubert, in *High Performance Devices, 2000. Proceedings 2000 IEEE/Cornell Conference on* (IEEE, Piscataway, NJ, 2000), pp. 168–172.
[9] S. J. Pearton *et al.*, J. Appl. Phys. **92**, 2047 (2002).
[10] A. Mintairov, J. Merz, A. Osinsky, V. Fuflyigin, and L. Zhu, Appl. Phys. Lett. **76**, 2517 (2000).
[11] T. Misaki, K. Tsuchiya, D. Sakai, A. Wakahara, H. Okada, and Y. A., Phys. Status Solidi C **0**, 188 (2000).
[12] T. Misaki, A. Wakahara, H. Okada, and A. Yoshida, Phys. Status Solidi C **0**, 2890 (2003).
[13] T. Misaki, A. Wakahara, H. Okada, and A. Yoshia, J. Cryst. Growth **260**, 1049 (2004).
[14] T. Cloitre, A. Sere, and R. L. Aulombard, Superlattices Microstruct. **36**, 377 (2004).
[15] S. Kikkawa and H. Morisaka, Solid State Commun. **112**, 513 (1999).
[16] R. Viennois, T. Taliercio, V. Potin, A. Errebbahi, B. Gil, S. Charar, A. Haidoux, and J.-C. Tédenac, Mater. Sci. Eng. B **82**, 45 (2001).
[17] K. Du, C. Bekele, C. C. Hayman, J. C. Angus, P. Pirouz, and K. Kash, J. Cryst. Growth **310**, 1057 (2008).
[18] S. Limpijumnong, S. N. Rashkeev, and W. R. L. Lambrecht, in *GaN and Related Alloys*, edited by S. J. Pearton, C. Kuo, A. F. Wright, and T. Uenoyama, Mater. Res. Soc. Proc. Vol. 537 (Materials Research Society, Warrendale, PA, 1999), p. G6.11.
[19] T. Misaki, X. Wu, A. Wakahara, and A. Yoshida, in *Proceedings of the International Workshop on Nitride Semiconductors, IPAP Conference Series*, Vol. 1 (Institute of Pure and Applied Physics, Tokyo, 2000), pp. 685–688.
[20] V. L. Shaposhnikov, A. V. Krivosheeva, F. Arnaud D'Avitaya, J.-L. Lazzari, and V. E. Borisenko, Phys. Status Solidi B **245**, 142 (2008).
[21] W. R. L. Lambrecht, E. Alldredge, and K. Kim, Phys. Rev. B **72**, 155202 (2005).
[22] T. R. Paudel and W. R. L. Lambrecht, Phys. Rev. B **76**, 115205 (2007).
[23] T. J. Peshek, T. R. Paudel, K. Kash, and W. R. L. Lambrecht, Phys. Rev. B **77**, 235213 (2008).
[24] T. R. Paudel and W. R. L. Lambrecht, Phys. Rev. B **78**, 115204 (2008).
[25] T. R. Paudel and W. R. L. Lambrecht, Phys. Rev. B **79**, 245205 (2009).
[26] T. R. Paudel, *Structure, Phonons and Related Properties in Zn-IV-$N_2$ (IV = Si, Ge, Sn), ScN and Rare-Earth Nitrides*, Ph.D. thesis, Case Western Reserve University, 2008.
[27] M. van Schilfgaarde, T. Kotani, and S. V. Faleev, Phys. Rev. B **74**, 245125 (2006).
[28] M. Methfessel, M. van Schilfgaarde, and R. A. Casali, in *Electronic Structure and Physical Properties of Solids. The Use of the LMTO Method*, Lecture Notes in Physics, Vol. 535, edited by H. Dreyssé (Springer-Verlag, Berlin, 2000), p. 114.
[29] T. Kotani and M. van Schilfgaarde, Phys. Rev. B **81**, 125117 (2010).
[30] J. P. Perdew, K. Burke, and M. Ernzerhof, Phys. Rev. Lett. **77**, 3865 (1996).
[31] M. van Schilfgaarde, T. Kotani, and S. Faleev, Phys. Rev. Lett. **96**, 226402 (2006).
[32] T. Kotani, M. van Schilfgaarde, and S. V. Faleev, Phys. Rev. B **76**, 165106 (2007).
[33] L. Hedin, Phys. Rev. A **139**, 796 (1965).
[34] L. Hedin and S. Lundqvist, in *Solid State Physics, Advanced in Research and Applications*, Vol. 23, edited by F. Seitz, D. Turnbull, and H. Ehrenreich (Academic Press, New York, 1969), pp. 1–181.
[35] F. Aryasetiawan and O. Gunnarsson, Phys. Rev. B **49**, 16214 (1994).
[36] M. Cardona and M. L. W. Thewalt, Rev. Mod. Phys. **77**, 1173 (2005).
[37] A. V. Rodina, M. Dietrich, A. Göldner, L. Eckey, A. Hoffmann, A. L. Efros, M. Rosen, and B. K. Meyer, Phys. Rev. B **64**, 115204 (2001).
[38] A. Alkauskas, P. Broqvist, and A. Pasquarello, Phys. Rev. Lett. **101**, 046405 (2008).
[39] K. Kim, W. R. L. Lambrecht, B. Segall, and M. van Schilfgaarde, Phys. Rev. B **56**, 7363 (1997).
[40] W. R. L. Lambrecht, A. V. Rodina, S. Limpijumnong, B. Segall, and B. K. Meyer, Phys. Rev. B **65**, 075207 (2002).